SUPPLEMENTARY METHODS

OSMOTIC STRESS EXPERIMENTS

Sample Preparation

Cholesterol (Chol), 1,2-dioleoyl-*sn*-glycero-3-phosphocholine (DOPC), 1,2-dipalmitoyl-*sn*-glycero-3-phosphocholine (DPPC), 1,2-distearoyl-*sn*-glycero-3-phosphocholine (DSPC), were purchased from Avanti Polar Lipids, Inc., Alabaster, AL, USA and used without further purification. After weighing, lipids were dissolved in chloroform/methanol 2:1 at a concentration of 10 mg/ml. These lipid stock solutions were mixed according to the molar ratios given in Table 1 and the organic solvent was then evaporated under a gentle nitrogen stream. To remove remaining solvent, the samples were placed in vacuum overnight. 18 MΩ/cm water (UHQ PS, USF Elga, Wycombe, UK) was added at 20 µl/mg lipid and the vials flushed with Ar, closed and taped to avoid oxidation. Fully hydrated multilamellar vesicles (MLVs) were obtained by keeping the samples at 50 °C for 4 hours with intermittent vortex mixing and freeze-thaw cycles. Polyethylene glycol (PEG 8000) from Fluka Chemie AG, Buchs, Switzerland was added at 0.0, 0.7, 1.4, 3.1, 4.9, 6.9, 11.8, 15.7, 23.7, 23.5 wt%. Osmotic pressures as a function of temperature and PEG concentration were calculated as detailed in Ref. [1].

Small-angle X-ray Diffraction (SAXD)

SAXD experiments were performed at the Austrian SAXS beamline (Elettra, Sincrotrone Trieste, Italy) using 8 keV photons and a mar300 (Marresearch, Norderstedt, Germany) image plate detector. Samples were filled into reusable quartz-glass capillaries and kept in a brass sample holder connected to a circulating water bath. The experiments were performed at T=15 °C for DOPC:DPPC:Chol and T=22 °C for DOPC:DSPC:Chol, at exposure times of 60 seconds. Silver behenate was used for angular calibration and the program FIT2D was used for angular integration of the 2D diffraction patterns.

The quality of the signal and background was not high enough to allow application of a full q-range analysis for deriving the structural membrane parameters as published earlier [2]. However, at least for medium and high PEG concentrations, four or more diffraction orders were discernible. This was enough to calculate electron density profiles using the integrated intensities of the peaks [2,3]. Therefore, electron densities were calculated using the standard Fourier synthesis

$$\rho = \sum_{h=1}^{h_{\max}} \alpha_h F_h \cos\left(\frac{2\pi h z}{d}\right), \qquad (1)$$

where α_h = ± 1 is the phase, d the lamellar repeat distance and F_h the form factor of the h^{th} diffraction order determined from Lorentzian fits to the Bragg peaks as $F_h = q\sqrt{I_h}$, ($q = 4\pi/\lambda \sin\theta$). The membrane thickness was defined as $d_B = d_{HH} + 10$ Å, where d_{HH} is the head-to-headgroup thickness, given by the position of maxima of the electron density profiles.

Estimates of bending rigidities from SAXD experiments

In order to estimate the bending rigidity K_C of the ternary mixtures, we analyzed the behavior of the water layer thickness $d_W = d - d_B$ with respect to osmotic pressure Π. The bilayer thickness d_B was assumed to remain constant. Analogous to Ref. [4], the function

$$\Pi = -\frac{A_{ham}}{6\pi}(d_W^{-3} - 2(d_W + d_B)^{-3} + (d_W + 2d_B)^{-3}) + P_h e^{-\frac{d_W}{\lambda_h}} + P_u e^{-\frac{d_W}{2\lambda_h}}, \qquad (2)$$

with $P_u = \frac{\pi k_B T}{32}\sqrt{P_h/K_C\lambda_h^3}$ was used to describe the measured data. The first term is the bilayer van der Waals attraction with the Hamaker coefficient A_{ham}, the second term corresponds to the hydration repulsion and the third term comes from bilayer undulations [5,6]. The Hamaker coefficient was fixed to the theoretical value of A_{ham}=4.3 zJ [7], leaving the three free parameters P_h, P_u and λ_h for least squares fitting.

The fact that Eq. (2) is linear in P_h and P_u , dramatically reduces the complexity of finding the global best fit. However, due to the significant reduction of bending fluctuations by cholesterol [8,9] determination of K_C for the present systems involves significant uncertainties, i.e. reasonable fits for Eq. (2) are obtained for a wide range of values of bending rigidities. In particular, K_C values for L_o phases are practically undetermined and we are limited to giving a lower limit of $K_C \geq 100$ k_BT. Figure S1 shows the fits to the L_d phases within the acceptable range of K_C values and for different sets of P_h, P_u and λ_h values (see, e.g. Ref. 10).

Molecular Dynamics (MD) Simulations

MD simulations using all-atom and Martini coarse-grained (CG) representations were performed on hydrated bilayers containing ternary mixtures of saturated lipid (either DPPC or DSPC), unsaturated lipid (DOPC) and cholesterol (Chol). DPPC-containing membranes were

simulated at mole fractions of 0.66:0.19:0.15 DOPC:DPPC:Chol (L_d phase) and 0.12:0.58:0.3 DOPC:DPPC:Chol (L_o phase), and at a temperature of T=15°C. DSPC-containing mixtures were studied at 0.74:0.09:0.17 DOPC:DSPC:Chol (L_d phase) and 0.12:0.56:0.32 DOPC:DSPC:Chol (L_o phase), and at a temperature of T=22°C. These particular conditions were chosen based on published phase diagrams of the respective mixtures [11,12].

All atom MD simulations (AA simulation set)

To design an all-atom (AA) representations of membranes with the desired lipid concentrations, model bilayers containing 400 lipids were constructed with the CHARMM-GUI Membrane Builder web tool [13]. The assembled membrane patches were solvated to a level of 40-50 waters/per lipid head-group. After initial energy minimization of 5400 steps, AA complexes were simulated using the CHARMM36 force field for lipids [14] and propagated for 100 ns using the NAMD modeling package (ver 2.9) [15]. Only the last 60ns trajectory segments, which were deemed as converged, were used for the analysis. The simulations were conducted in the constant temperature and pressure (NPT) ensemble with semi-isotropic pressure coupling and utilizing Particle-Mesh-Ewald (PME) for long-range electrostatics. The Nose-Hoover Langevin piston method was used to control the target 1atm pressure with the Langevin piston period set to 100 fs and Langevin piston decay set to 50 fs. All MD simulations were performed with rigid bonds allowing a 2 fs time step. While the detailed structural characterization of the lipid membranes simulated with the AA representations is subject for a separate article (manuscript in preparation), here we illustrate the well-converged behavior of the simulated systems by plotting in Figure S6 the time-evolution of the area per molecule from the different AA trajectories. The convergence can be assessed from near-flat profiles (within fluctuations).

MD simulations with Martini CG force-fields (MS and ML simulation sets)

Martini CG simulations of DOPC/DPPC/Chol and DOPC/DSPC/Chol mixtures with appropriate lipid fractions were conducted on two sets of differently sized bilayer patches. As listed in Table 1 of the main text, we studied complexes consisting of 512 lipids in total (designated as the MS simulation set), and larger bilayers, containing 2048 lipids (ML simulation set).

For MS simulations, bilayers containing 512 molecules with appropriate lipid compositions were built from an equilibrated CG DOPC bilayer patch which contained 128 lipids (available for download from the Martini website, http://md.chem.rug.nl/cgmartini/). This small patch was replicated in the x-y bilayer plane directions to yield 512-lipid size membrane,

and the desired lipid compositions were then created by random replacement of an appropriate number of lipids. The MS systems were simulated for 18-20 μs (last 16-18 μs trajectory intervals being used for analysis, see Table 1) using the Martini CG force field for lipids [16] and Gromacs software [17] version 4.5.5. The simulations were run in the *NPT* ensemble under the semi-isotropic pressure conditions. Temperature and pressure were controlled using the Berendsen weak coupling algorithm [18]. τ_P=1.1 ps time constant and compressibility of $1e^{-6}$ bar^{-1} were used. The neighbor list cut-off was set to 1.4 nm allowing for 30 fs time-step. The time courses of the area per molecule from different trajectories in the MS set are presented in Figure S7. They show flat, within fluctuations, profiles indicating convergence of the simulations.

The large-size bilayers for ML simulation set were built by replicating the last membrane configurations from the respective MS simulations in x-y bilayer plane. The resulting 2048-lipid bilayers, after relatively short (300ns) initial equilibration, were subjected to 6 μs of MD. These runs were performed under the same conditions as the MS simulations.

Calculation of tilt and splay modulii from simulations

We have previously described the procedure for calculating the tilt and splay moduli, χ and χ_{12} respectively, for lipids and sterols from MD simulations [19,20]. Briefly, we first define local lipid director vectors $\vec{t}$ in the following manner (see Fig. S1): for PC lipids in the all-atom representation, $\vec{t}$ is the vector that connects the midpoint between the phosphate and backbone C2 atoms to the geometric center-of-mass of the three terminal carbons on the two lipid chains; in CG Martini simulations, $\vec{t}$ for lipids is defined as the vector connecting the geometric center-of-mass of PO4, GL1 and GL2 beads with the geometric center-of-mass of the terminal carbon beads on the two lipid tails. For cholesterol, in all-atom representation the director vector joins C3 and C17 atoms, and in the CG description $\vec{t}$ connects R1 and R5 ring beads.

The tilt angle, θ, between $\vec{t}$ vector and the bilayer normal direction is defined In the range [0°; 180°] so that θ=0 represents a local orientation where $\vec{t}$ is parallel to the bilayer normal z axis. To calculate, for example, the cholesterol tilt modulus, the normalized probability density $P(\theta)$ of the tilt angle representing the local direction of Chol ring plane with respect to bilayer normal was constructed for each simulated system. The $P(\theta)$ distribution was obtained by creating an orientational angle histogram in the angular range [0°; 90°]. A quadratic fit was performed to an expression of the form $-k_B T \ln\left[P(\theta)/\sin\theta\right]$ over the angular interval chosen to represent the best-sampled angular region and at the same time to limit the fit to the low θ regime where the quadratic expansion of the free energy with respect to tilt is valid [21]. For the L_o phase mixtures, the angular range for fitting was $\theta \in [5;20]$, and for Ld phase - $\theta \in [10;30]$

(see Figure 1 in the main text). Finally, χ was determined from the coefficient that corresponded to the best fit.

Using the same director vector definitions, the splay modulus for a particular pair of molecules was calculated by defining a splay angle, α, between $\vec{t}$ vectors and constructing $P(\alpha)$ probability distributions. Limiting the analysis to pairs for which at least one of the participant molecules is tilted by no more than θ=10° angle with respect to the bilayer normal, χ_{12} can be obtained from $P(\alpha)$ distributions by performing a quadratic fit in the interval of small α angles to $-k_B T \ln\left[P(\alpha)/\sin\alpha\right]$ function. Again, $\alpha \in [5;20]$ and $\alpha \in [10;30]$ angular ranges for L_o and L_d phase mixtures, respectively, were used for fitting, and χ_{12}-s corresponded to the coefficients allowing the best fit.

The above described procedures were used to determine tilt and splay modulii from AA and MS sets of simulations.

Spectral analysis method for calculation of bilayer bending modulus from MD Simulations

The bending modulus was calculated from the ML simulations (for 2048-lipid size bilayers) using the spectral analysis method [22]. This technique uses the Helfrich continuum representation for lipid bilayer undulations $u(x,y)$, and expands the Hamiltonian of the fluctuating membrane to lower order terms in $u(x,y)$ [23]:

$$H[u(x,y)] = \frac{1}{2}\iint\left[K_C\left|\nabla^2 u(x,y)\right|^2 + \gamma\left|\nabla u(x,y)\right|^2\right]dxdy \qquad (3)$$

Here the two terms represent bending and surface tension contributions, with their respective K_C and γ constants. Analysis of the bending rigidity from the bilayer undulations is most conveniently performed in Fourier space using the expansion (see Ref. [22] , for example):

$$u(\vec{r}) = \sum_{\vec{q}} u(q) e^{i\vec{r}\cdot\vec{q}} \qquad (4)$$

Where $\vec{r} = (x,y)$ and $\vec{q} = (q_x, q_y)$ denote two-dimensional real space and reciprocal space vectors, respectively. Assuming a tensionless membrane, the spectral amplitude profile $\langle u^2(q)\rangle$ for the small-q modes can be obtained from the equipartition theorem as: $(k_B T / A_{BOX}) \times K_C \times q^{-4}$, where A_{BOX} represents the lateral area of the simulation box.

In addition, as has been detailed elsewhere [22,24], local protrusion modes in $\langle u^2(q)\rangle$ can also be observed in high q-regime. Governed by the microscopic protrusion tension, γ_P, such modes can be approximated by $(k_B T / A_{BOX}) \times \gamma_P^{-1} \times q^{-2}$. Thus, the full spectrum of the $\langle u^2(q)\rangle$ amplitudes is expected to contain the two q^{-4} and q^{-2} regimes, corresponding to the small and high wavevector modes respectively.

The last 6 μs segments of ML trajectories were analyzed for wavevector-dependent undulatory modes by representing the position of each bilayer leaflet using the vertical z-coordinates of lipid backbone GL1 and GL2 CG beads. Following the procedure outlined in our earlier work [25], the resulting traces for two monolayers were then subjected to interpolation with spline functions of the fifth order to yield smooth leaflet shapes. Application of a two-dimensional Fourier transform to the smoothed monolayer shapes yielded undulatory spectral amplitudes, which were subsequently time-averaged and converted into histograms according to wavevector magnitude, q. The calculated Fourier amplitudes $\langle u^2(q) \rangle$ presented here for all simulated bilayers were scaled by the lateral area of the respective simulated systems, A_{BOX}, and the values for K_C were obtained from the fitting coefficients to the q^{-4} function (see Figure S8).

Estimation of error bars for calculated bending rigidity using the splay angle distribution methodology

We considered several approaches to estimate uncertainties for the parameters presented in Figure 2 and Table 2 (in the main text) as well as in Table S1 in the Supplemental Material. In the first approach, the fitting procedure to estimate the splay modulus was conducted on the $P(\alpha)$ distributions obtained from the complete trajectories (see Table 1 for the lengths of the trajectories), as well as from splitting the analysis trajectory into two equal parts. In all cases the angular interval was kept the same ($\alpha \in [5;20]$ and $\alpha \in [10;30]$ angular intervals for the L_o and L_d systems, respectively). Error bars for each splay modulus parameter were obtained from the corresponding standard deviations.

In the second approach, we first analyzed the complete trajectories and obtained fits again in $\alpha \in [5;20]$ and $\alpha \in [10;30]$ angular intervals for the L_o and L_d systems, respectively. To estimate errors, we then repeated the fitting procedure on the same trajectories by considering smaller angular windows within the intervals where the original fit was obtained ($\alpha \in [5;20]$ or $\alpha \in [10;30]$), and calculated standard deviations from the fits obtained by "sliding" the fitting windows. For example, if the original fit was performed in the $\alpha \in [10;30]$ range, we defined 10^o or 15^o angular intervals and performed fits in [10:20], [12:22], …, [20:30] and [10:25], [11: 24], …etc, [15:30] ranges.

From these different considerations, we evaluated the uncertainties obtained, and chose to report throughout the manuscript the *highest* limit of the error bars obtained from different error estimate approaches. Lastly, since the obtained values for the splay moduli relate to *monolayer* bending rigidity, we set error bars on the bilayer bending rigidity values (in Table 2) as $\sqrt{2} \times \sigma_{err}$, where σ_{err} was the uncertainty in the monolayer bending constant.

REFERENCES

(1) Stanley, C. B.; Strey, H. H. *Macromolecules* **2003**, *36*, 6888.

(2) Pabst, G.; Rappolt, M.; Amenitsch, H.; Laggner, P. *Phys Rev E Stat Phys Plasmas Fluids Relat Interdiscip Topics* **2000**, *62*, 4000.

(3) Rappolt, M. *Journal of Applied Physics* **2010**, *107*, 084701.

(4) Pabst, G.; Boulgaropoulos, B.; Gander, E.; Sarangi, B. R.; Amenitsch, H.; Raghunathan, V. A.; Laggner, P. *J Membr Biol* **2009**, *231*, 125.

(5) Parsegian, V. A.; Rand, R. P. Interaction in membrane assemblies. In *Structure and Dynamics of Membranes*; Lipowsky, R., Sackmann, E., Eds.; Elsevier: Amsterdam, 1995; pp 643.

(6) Podgornik, R.; Parsegian, V. A. *Langmuir* **1992**, *8*, 557.

(7) Podgornik, R.; French, R. H.; Parsegian, V. A. *Journal of Chemical Physics* **2006**, *124*, 044709.

(8) Hodzic, A.; Rappolt, M.; Amenitsch, H.; Laggner, P.; Pabst, G. *Biophys J* **2008**, *94*, 3935.

(9) Pan, J.; Tristram-Nagle, S.; Nagle, J. F. *Phys Rev E Stat Nonlin Soft Matter Phys* **2009**, *80*, 021931.

(10) Tristram-Nagle, S.; Petrache, H. I.; Nagle, J. F. *Biophys J* **1998**, *75*, 917.

(11) Heberle, F. A.; Wu, J.; Goh, S. L.; Petruzielo, R. S.; Feigenson, G. W. *Biophys J* **2010**, *99*, 3309.

(12) Uppamoochikkal, P.; Tristram-Nagle, S.; Nagle, J. F. *Langmuir* **2010**, *26*, 17363.

(13) Jo, S.; Lim, J. B.; Klauda, J. B.; Im, W. *Biophysical Journal* **2009**, *97*, 50.

(14) Klauda, J. B.; Venable, R. M.; Freites, J. A.; O'Connor, J. W.; Tobias, D. J.; Mondragon-Ramirez, C.; Vorobyov, I.; MacKerell, A. D.; Pastor, R. W. *Journal of Physical Chemistry B* **2010**, *114*, 7830.

(15) Phillips, J. C.; Braun, R.; Wang, W.; Gumbart, J.; Tajkhorshid, E.; Villa, E.; Chipot, C.; Skeel, R. D.; Kale, L.; Schulten, K. *Journal of Computational Chemistry* **2005**, *26*, 1781.

(16) Marrink, S. J.; Risselada, H. J.; Yefimov, S.; Tieleman, D. P.; de Vries, A. H. *J Phys Chem B* **2007**, *111*, 7812.

(17) Hess, B.; Kutzner, C.; van der Spoel, D.; Lindahl, E. *Journal of Chemical Theory and Computation* **2008**, *4*, 435.

(18) Berendsen, H. J.; Postma, J. P. M.; DiNola, A.; Haak, J. R. *Journal of Chemical Physics* **1984**, *81*, 3684.

(19) Khelashvili, G.; Harries, D. *J Phys Chem B* **2013**, *117*, 2411.

(20) Khelashvili, G.; Pabst, G.; Harries, D. *J Phys Chem B* **2010**, *114*, 7524.

(21) Kessel, A.; Ben-Tal, N.; May, S. *Biophysical Journal* **2001**, *81*, 643.

(22) Lindahl, E.; Edholm, O. *Biophys J* **2000**, *79*, 426.

(23) Helfrich, W. *Z Naturforsch C* **1973**, *28*, 693.

(24) Brandt, E. G.; Braun, A. R.; Sachs, J. N.; Nagle, J. F.; Edholm, O. *Biophysical Journal* **2011**, *100*, 8.

(25) Khelashvili, G. R., M.; Chiu, S.-W.; Pabst, G.; Harries, D. *Soft Matter* **2011**, *7*, 10299.

SUPPLEMENTARY TABLES

Table S1: Bilayer bending modulus ($K_{C,}$ in k_BT units) for DOPC/DSPC/Chol mixtures in L_d and L_o phases obtained from the Martini simulations of bilayer patches containing 512 lipids (MS simulation set in the main text) or 128 lipids [a]

SYSTEM	Martini (512 lipids)	Martini (128 lipids)
DOPC/DSPC/Chol Ld	24 ± 3	25 ± 1
DOPC/DSPC/Chol Lo	89 ± 4	88 ± 4

[a] – For adequate sampling, the simulation times for 128 lipid-size bilayers were 20 μs.

SUPPLEMENTARY FIGURES

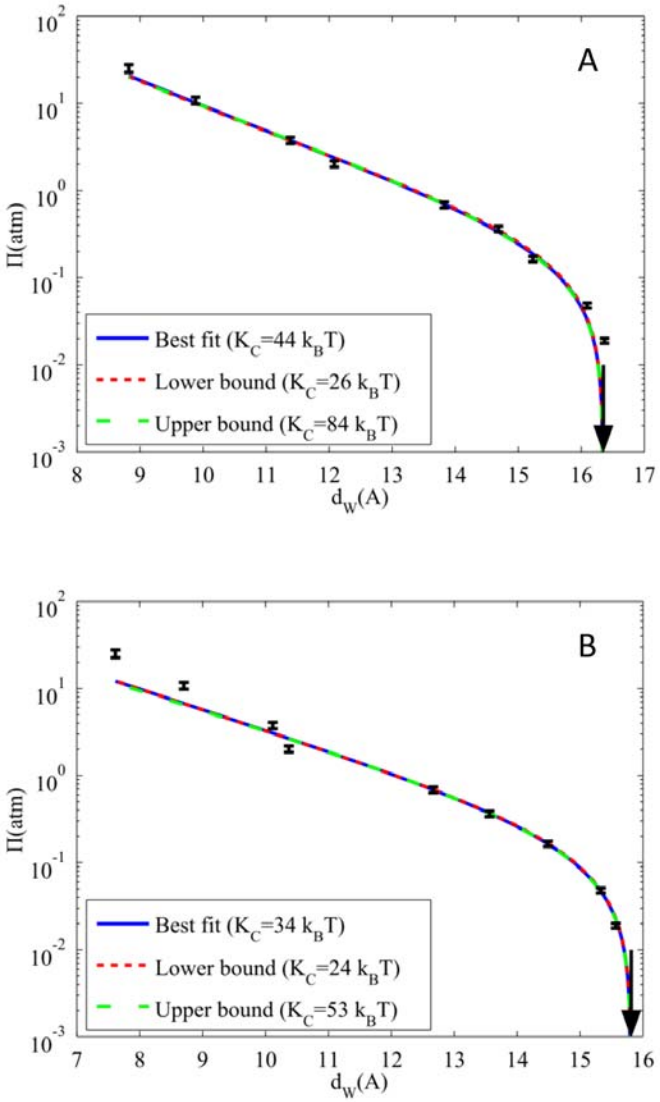

Figure S1: Bilayer separation d_W as a function of osmotic pressure Π for L_d domains of DOPC/DPPC/Chol (panel ***A***) and DOPC/DSPC/Chol (panel ***B***), respectively. Blue solid lines confer to best fits, red broken lines to the lower boundary of acceptable K_C and green broken lines to the upper boundary. For DOPC/DPPC/Chol, results for the hydration parameters are P_h = 13263 atm, λ_h=1.32 Å for K_C = 44 k_BT, P_h = 18206 atm, λ_h= 1.22 Å for K_C = 26 k_BT and P_h = 7359 atm, λ_h= 1.47 Å for K_C = 84 k_BT. For DOPC/DSPC/Chol, P_h = 1116 atm, λ_h= 1.68Å for K_C = 34 k_BT, P_h = 1335 atm, λ_h= 1.58 Å for K_C = 24 k_BT and P_h = 830 atm, λ_h= 1.82 Å for K_C = 53 k_BT.

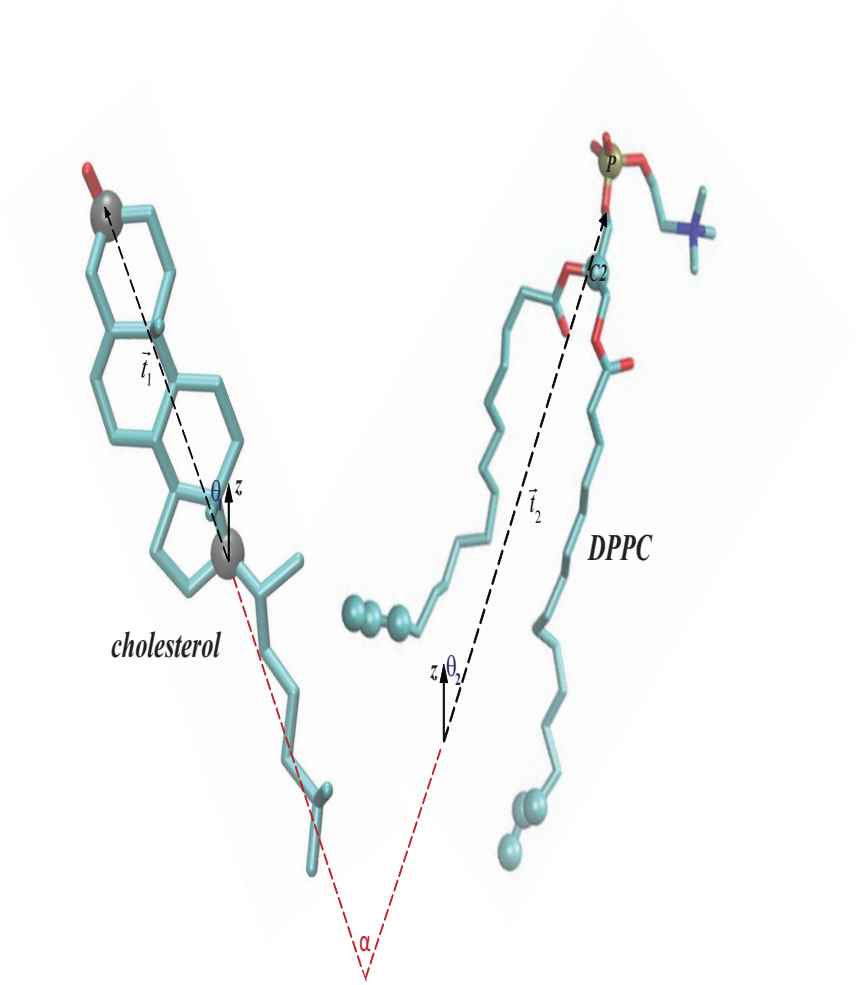

Figure S2: Schematic representation of cholesterol/DPPC lipid pair (in licorice representation) showing the definitions used for tilt and splay modulii calculations. The vectors $\vec{t}_1$ and $\vec{t}_2$ describe the orientations of Chol and DPPC lipid, respectively, with respect to the bilayer normal z axis (shown as horizontal vector). $\vec{t}_1$ connects C3-C17 atoms on the Chol ring plane (depicted as grey spheres). The vector $\vec{t}_2$ connects the mid-point between the head-group phosphate atom (golden sphere), and the backbone C2 atom (cyan sphere in the lipid backbone area) with the center-of-mass of the three terminal carbon atoms on the lipid tails (six cyan spheres in the hydrocarbon chains). θ_1 and θ_2 denote the respective tilt angles for $\vec{t}_1$ and $\vec{t}_2$ vectors, and α is the splay angle between the two vectors.

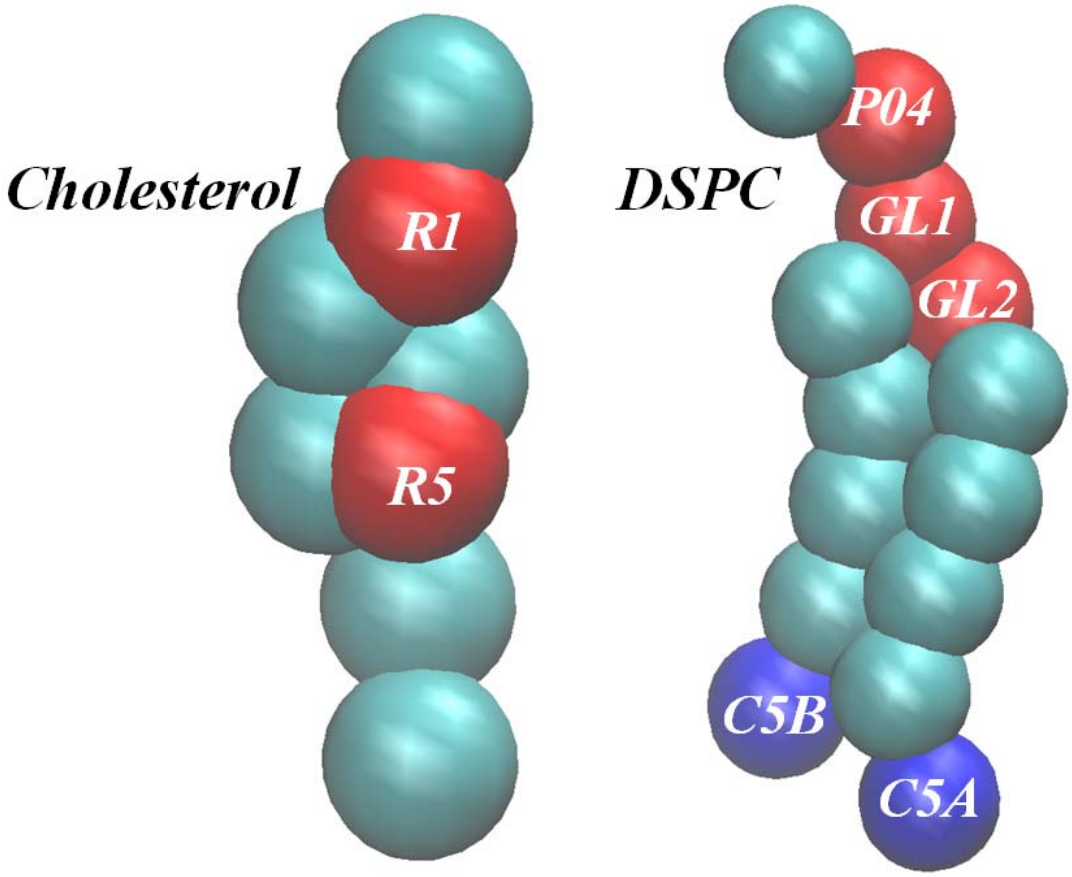

Figure S3: Martini representation of cholesterol and DSPC lipid, highlighting location of beads (PO4, GL1, GL2, C5A, C5B in DSPC, and R1 and R5 in Chol) used for defining the director vectors.

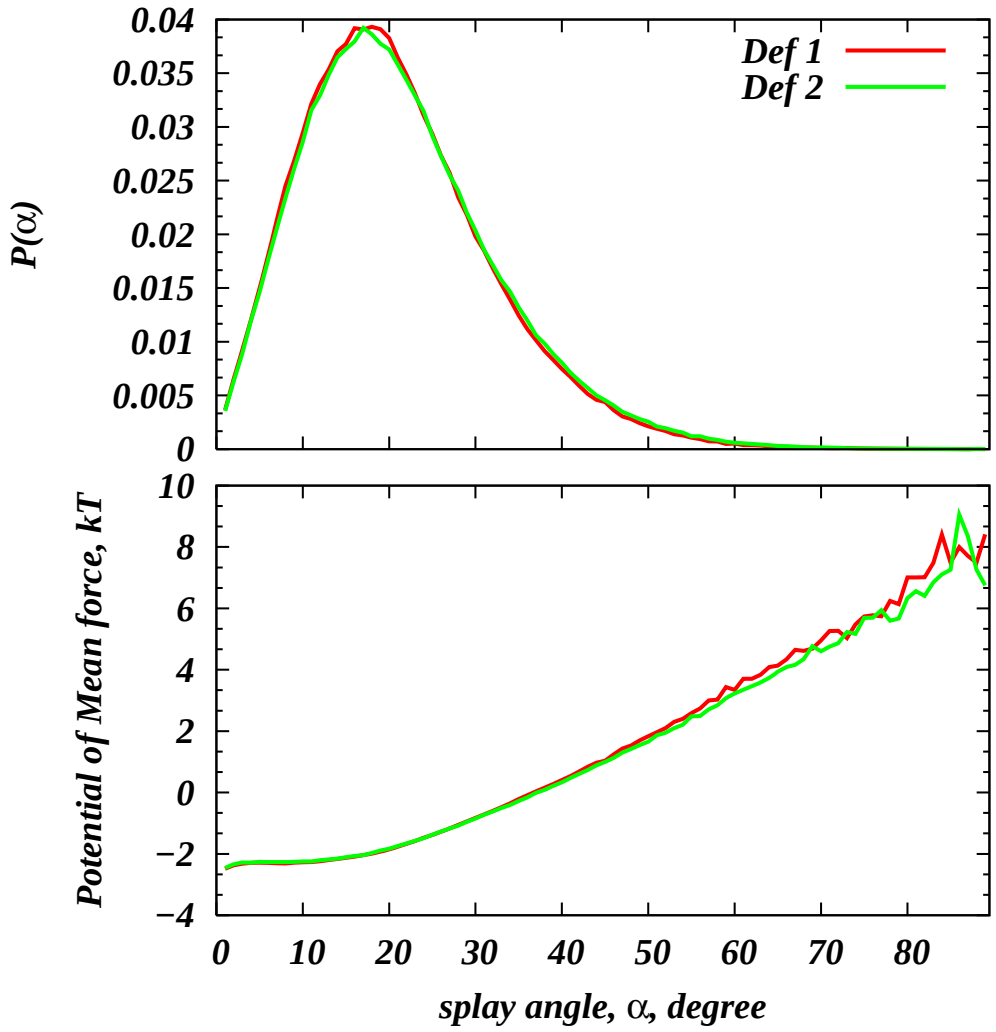

Figure S4: Normalized probability densities $P(\alpha)$ (*upper panel*) of finding a pair of DOPC lipids at an angle α with respect to each other and the resulting potential of mean force profiles (*lower panel*). The data shown is obtained from Martini simulations of DOPC/DSPC/Chol mixtures in the L_d phase (MS simulation set in Table 1) using two different definitions for the vector director: Def 1 connects the geometric center-of-mass of PO4, GL1 and GL2 beads with the geometric center-of-mass of the terminal carbon beads on the two lipid tails (definition employed in the main text); Def 2 joins the center-of-mass of the entire head-group of the lipid with the center-of-mass of the terminal carbon beads on the two lipid tails. The splay modulus values obtained from the two definitions are within 2% of each other.

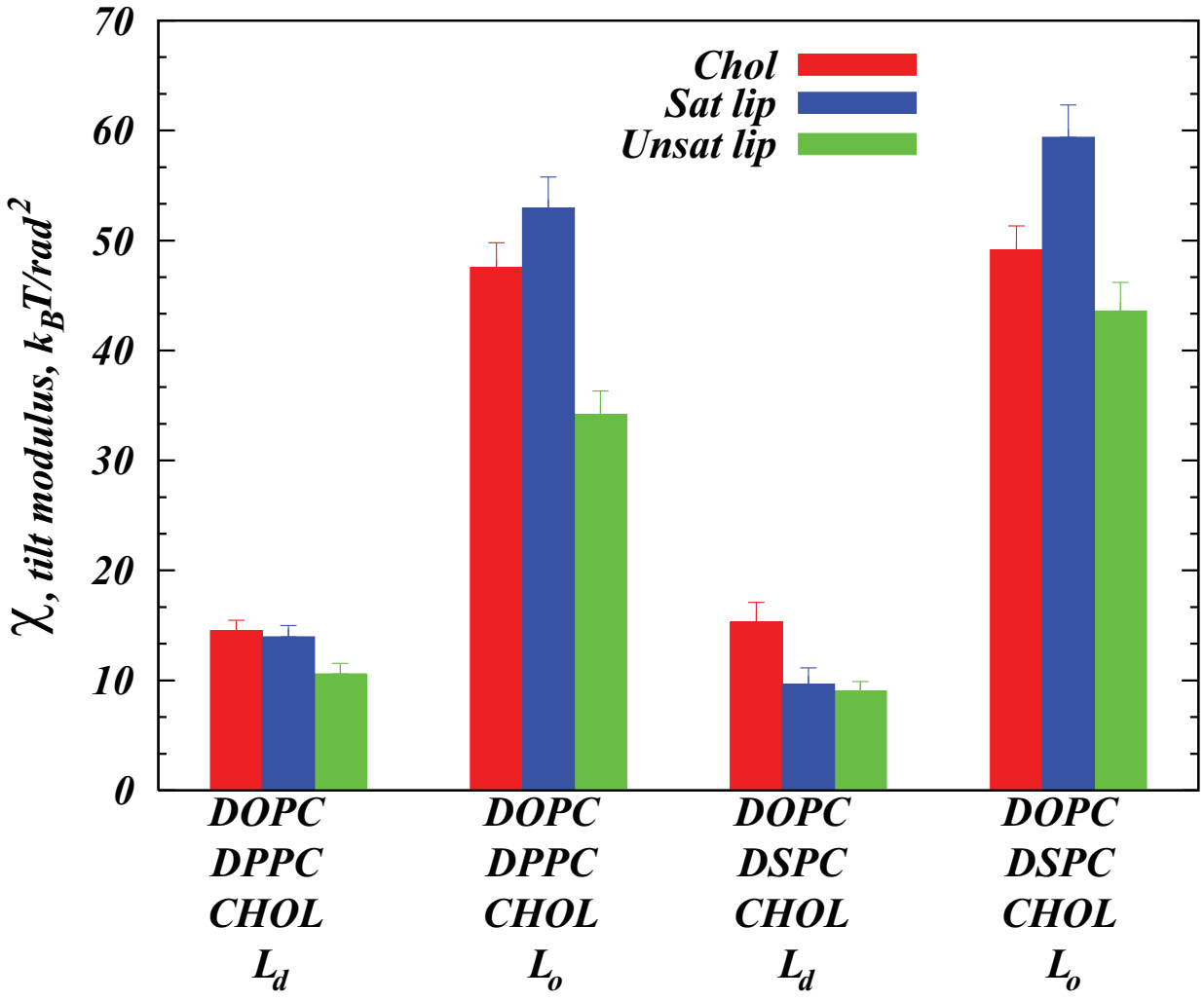

Figure S5: Tilt modulii χ for Cholesterol (red), saturated lipid (blue), and unsaturated lipid (green) from AA simulations of DOPC/DPPC/Chol and DOPC/DSPC/Chol mixtures in L_d and L_o phases (AA simulation set in Table 1). The error-bars were calculated from the standard deviations obtained from the fits performed for different angular intervals, as described in the Supporting Information, above.

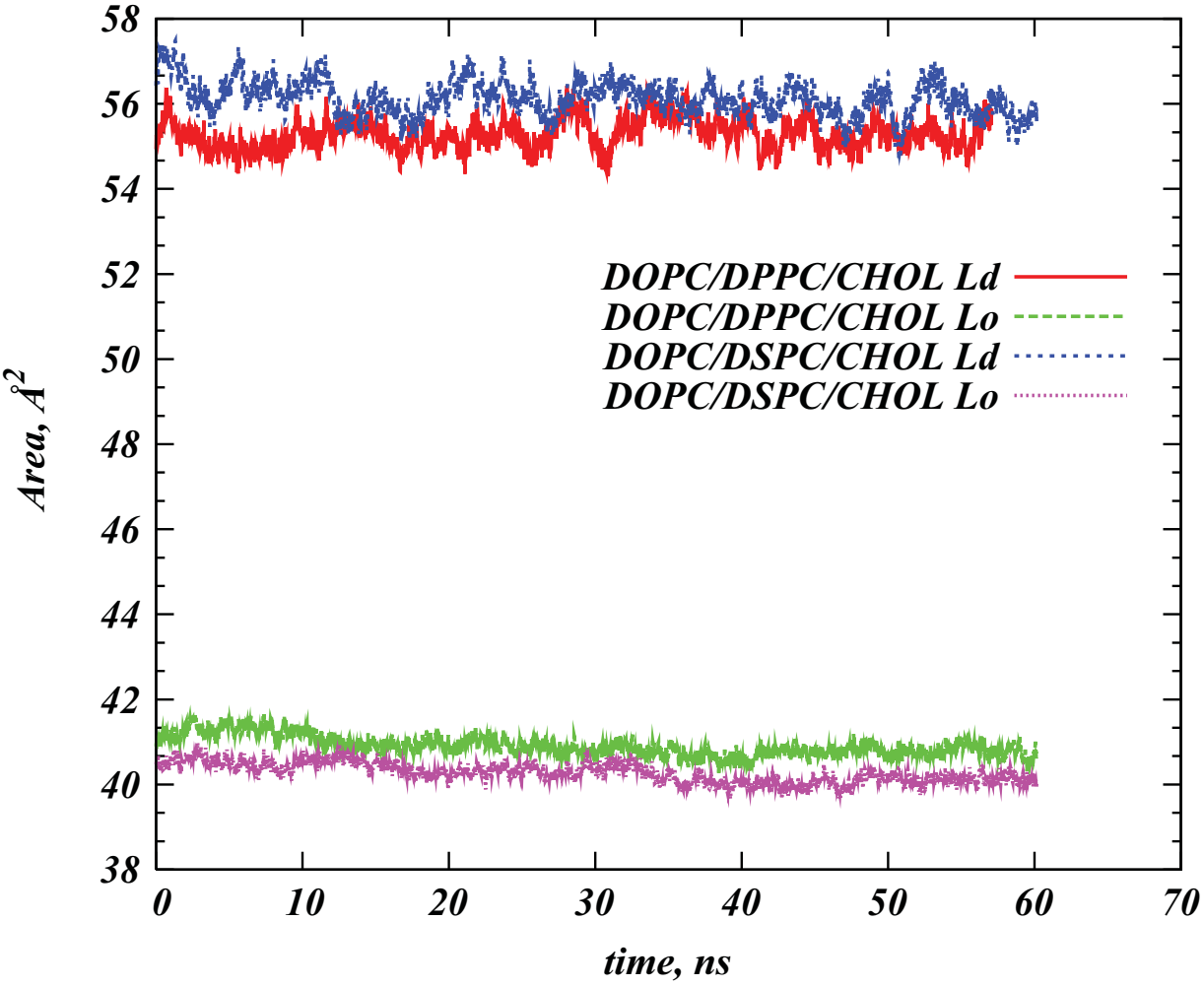

Figure S6: Time-evolution, after initial equilibration, of the area per molecule in the trajectories of the different AA simulations. The convergence is illustrated from near-flat within fluctuation profiles. These converged segments were used for the analyses presented.

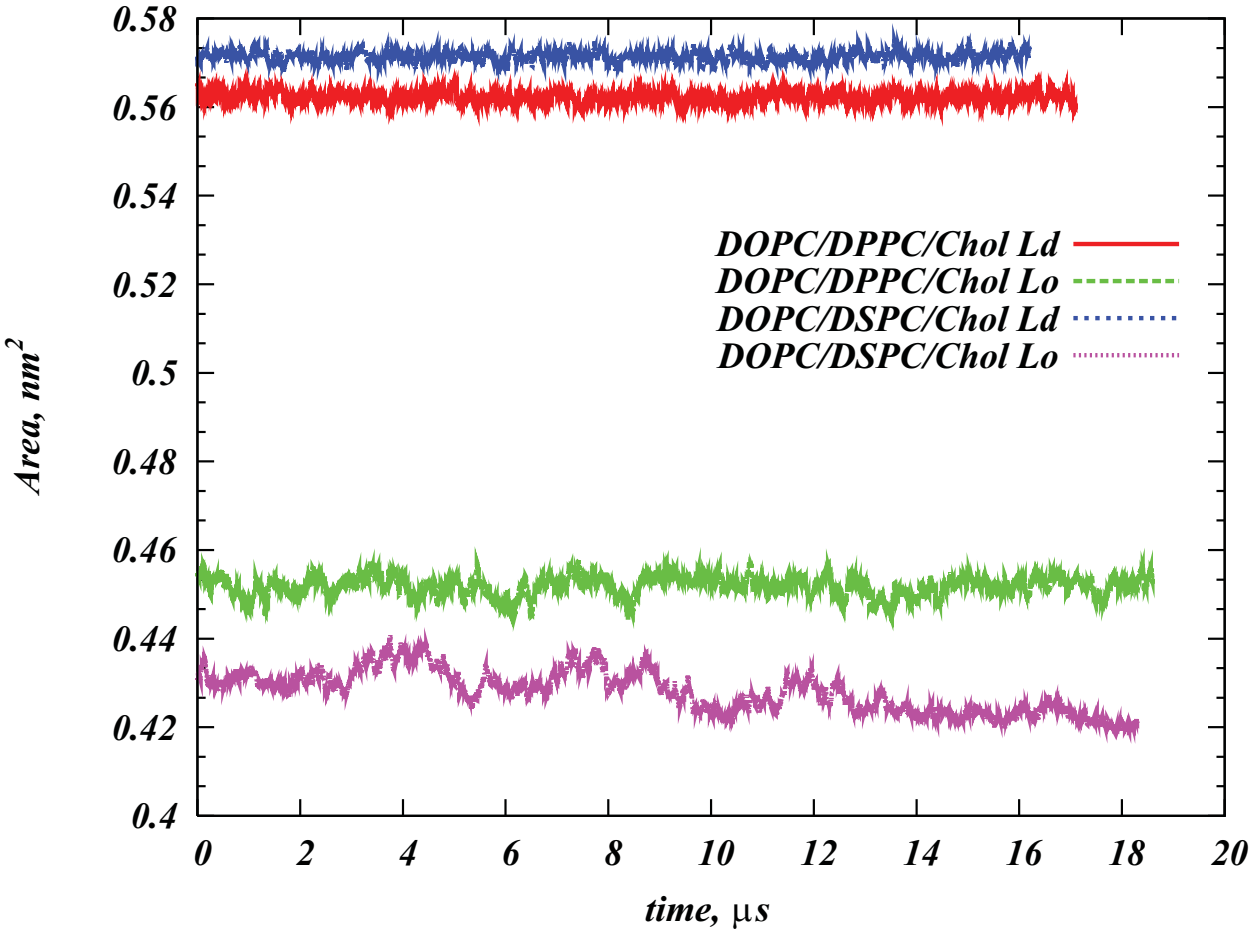

Figure S7: Time-evolution, after initial equilibration, of the area per molecule in the trajectories of the different MS simulations. The convergence is illustrated from near-flat within fluctuation profiles. These converged segments were used for the analyses presented.

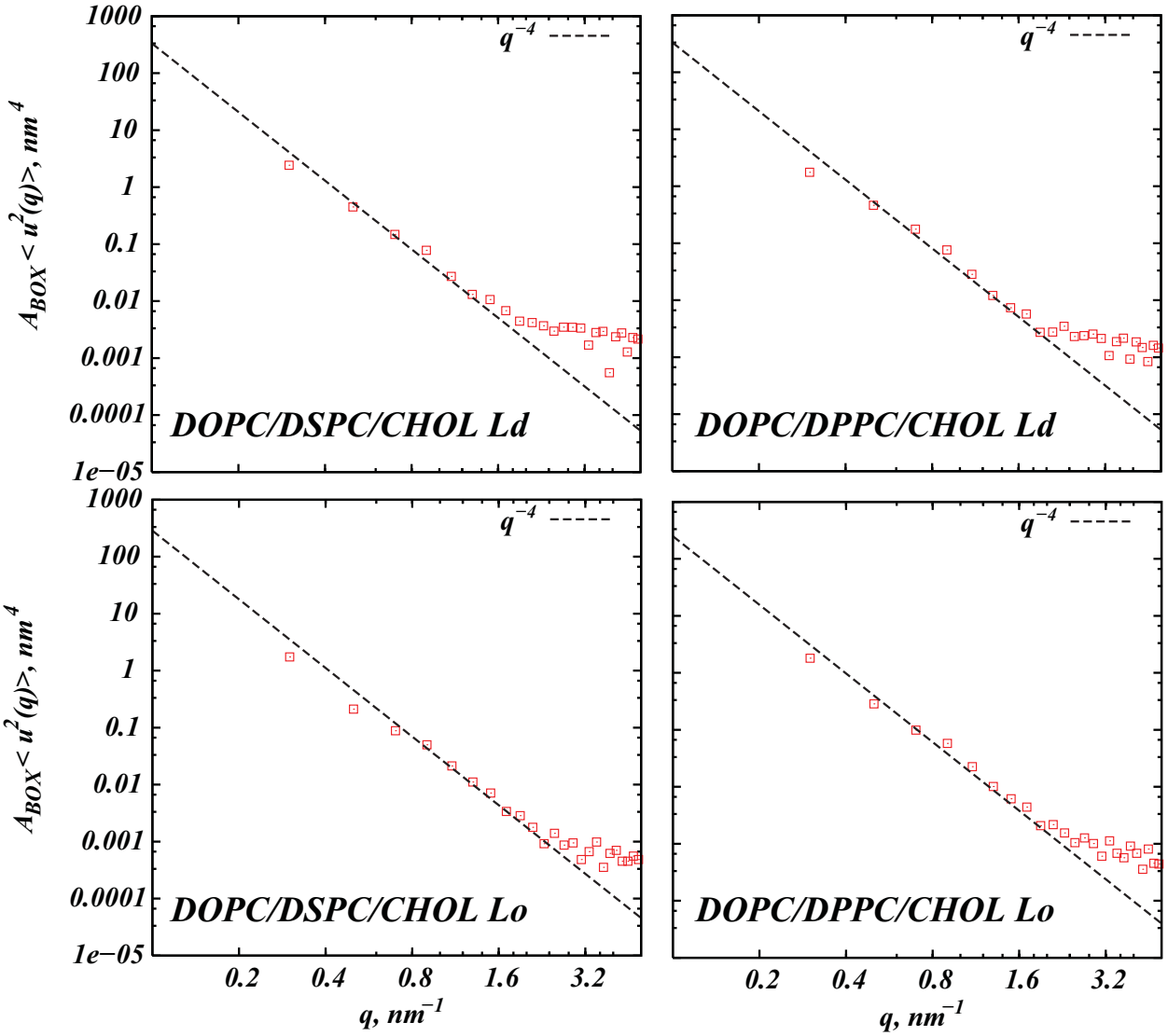

Figure S8: Spectral analysis on the trajectories from the ML simulations. Shown, for DOPC/DPPC/Chol and DOPC/DSPC/Chol mixtures in L_d and L_o phases, on the logarithmic scale is the dependence of the product of the average simulation box size (A_{BOX}) and the spectral amplitude (<$u^2(q)$>) on the wave number (q). The lines on each panel represent q^{-4} fits to the data in the low q regime. The values for K_C were obtained from the fitting coefficients to the q^{-4} functions.